Journal of Fluids and Structures (2002) **16**(3), 317–329
doi:10.1006/jfls.2001.0423, available online at http://www.idealibrary.com on IDEAL®

THE STRUCTURE OF TURBULENT SHEAR FLOW AROUND A TWO-DIMENSIONAL POROUS FENCE HAVING A BOTTOM GAP

H. B. Kim and S. J. Lee

Department of Mechanical Engineering, Pohang University of Science and Technology Pohang 790-784, Korea

(Received 9 May 2000, and in final form 21 September 2001)

The flow field behind porous fences of geometric porosity $\varepsilon = 38{\cdot}5\%$ with various bottom gaps (G) has been investigated using a hybrid PTV velocity field measurement technique. Four gap ratios $G/H = 0{\cdot}0, 0{\cdot}1, 0{\cdot}2$ and $0{\cdot}3$ were tested in this study. One thousand instantaneous velocity vector fields in the x–y plane were consecutively measured for each gap ratio. The free-stream velocity was fixed at 10 cm/s and the corresponding Reynolds number based on the fence height (H) was $\mathrm{Re} = 2\,985$. The results show that the gap ratio $G/H = 0{\cdot}1$ gives the best shelter effect among the four gap ratios tested in this study, having a small shelter parameter ψ in a large area behind the fence. As the gap ratio increases, the region of mean velocity reduction decreases and the lower shear layer developed from the bottom gap expands upward. From the spatial distributions of turbulence statistics including turbulence intensities, Reynolds shear stress and turbulent kinetic energy, the wake characteristics can be divided into two categories depending on the gap ratio. When the gap ratio is above $G/H = 0{\cdot}2$, the turbulence statistics have large values in the lower shear layer. For the gap ratio $G/H \leq 0{\cdot}1$, however, the lower shear layer displays small turbulence-statistics values and approach those of the no-gap case ($G/H = 0$) with increasing distance downstream. In the upper shear layer separated from the fence top, the turbulence statistics are nearly independent of the gap ratio.

1. INTRODUCTION

Porous fences have been widely used as manipulators to control an oncoming flow. In previous studies on porous fences, the fence porosity was found to be the most important parameter determining the flow characteristics around porous fences. Many studies have focused on the reduction of the mean velocity in the wake behind a porous fence and measured the drag force acting on the fence with varying fence porosity. Since a surface-mounted vertical fence results in a complex flow around the fence, much attention has been paid to the basic physics of the wake flow. In this work, we studied in detail the flow structure in the region just behind the fence. Porous fences have been used as partial screens, not only to reduce the flow velocity but also to control the turbulence structure. For example, a line of trees along a shore reduces the mean velocity and turbulence level of an approaching high-speed wind.

Raine & Stevenson (1977) measured the mean velocity and turbulence intensity profiles of the wake behind various porous fences embedded in an atmospheric boundary layer using a hot-wire anemometer. They classified the wake flow into two regions: the bleed-flow-dominant region and the displacement-flow region. However, the hot-wire measurements could not detect the reverse flow immediately behind the fence and underestimated the turbulence intensities in this region.

0889–9746/02/030317 + 13 $35.00/0

Perera (1981) employed a pulsed-wire anemometer (PWA) system to resolve the shortcomings of the hot-wire measurement. In his study, the fence porosity was found to be the most influential parameter affecting the wake characteristics behind the fence, compared with other factors that can be considered in fence design.

Castro (1971) revealed that there was no vortex street behind a porous plate for which the fence porosity was greater than 30%. This means that a recirculation region is not formed behind a plate when the porosity is larger than 30%. Perera (1981) found similar results.

However, the near wake just behind these fences has received relatively little attention because of its complex flow structure that is characterized by high shear rate, large pressure gradient and high turbulence intensity. Lee & Kim (1999) measured the mean velocity field of flow behind a porous fence for various fence porosities (ε) using the 2-frame particle tracking velocimetry (PTV) technique (Baek & Lee 1996). In their study, the $\varepsilon = 20\%$ porous fence showed the largest velocity reduction in the near wake region. However, the 40% porous fence had smaller turbulence intensities in the shear layer separated from the top of fence than the $\varepsilon = 20\%$ porous fence. Kim & Lee (2001) investigated the effect of hole diameter on the wake behind porous fences with the same porosity of $\varepsilon = 38{\cdot}5\%$.

When a long wind fence is constructed, roads and pipelines create a gap between the bottom of the fence and the ground. In addition, the sheltering effect of a line of trees can be simulated as a fence with a bottom gap at the ground surface. Cho (1996) briefly investigated the wake flow behind a two-dimensional porous fence with a bottom gap. He found that a wind fence with a bottom gap was cost-effective in reducing the surface shear stress in the far wake region. However, this study was too limited to fully understand the effect of fence gap on the flow characteristics of the near wake behind a porous fence.

In the present study, the flow structure of the near wake behind a porous fence with a bottom gap has been investigated experimentally using a varying gap ratio. For each porous fence with a different value of the bottom gap, 1 000 instantaneous velocity fields in the x–y plane were measured using a hybrid PTV method (Kim & Lee 2000) and statistically averaged to get the spatial distributions of the mean velocity and turbulence statistics of the near wake.

2. EXPERIMENTAL APPARATUS AND PROCEDURE

The experiments were carried out in a circulating water channel with a test section of width $\times$ height $\times$ length $= 300 \times 200 \times 1\,200$ mm. A schematic diagram of the experimental set-up and the coordinate system used in this study are shown in Figure 1.

The model fence was constructed from stainless steel of 0.6 mm thickness (B). The fence had a height (H) of 30 mm and a flat end at the fence top. The aspect ratio (W/H) and shape ratio (B/H) were 10 and 0·02, respectively. The model fence was installed 40 cm downstream from the inlet of the test-section. The gap between the fence and the bottom plate was varied over the values $G = 0$, 3, 6 and 9 mm. Circular holes of 2·1 mm diameter were chemically etched to have a geometric porosity (ε) of 38·5% in a tetragonal pattern and this porosity was found to give rise to small turbulence intensities and a large mean velocity reduction (Lee & Kim 1999). Figure 1(b) shows the mean velocity profiles measured at the upstream location of $x/H = -0{\cdot}5$ without the fence. The boundary layer thickness (δ) at the fence location was approximately $\delta/H \approx 0{\cdot}18$. The free-stream velocity was fixed at $U_0 = 10$ cm/s and the corresponding Reynolds number based on the fence height H was approximately 2 985.

The surface pressure variations at $x/H = -3$, -2, $-1{\cdot}5$ and -1 were measured along the channel center ($z/H = 0$) and side ($z/H = \pm 0.5$) planes for the $G/H = 0$ case. One hundred thousand pressure-data points were collected from each pressure transducer at

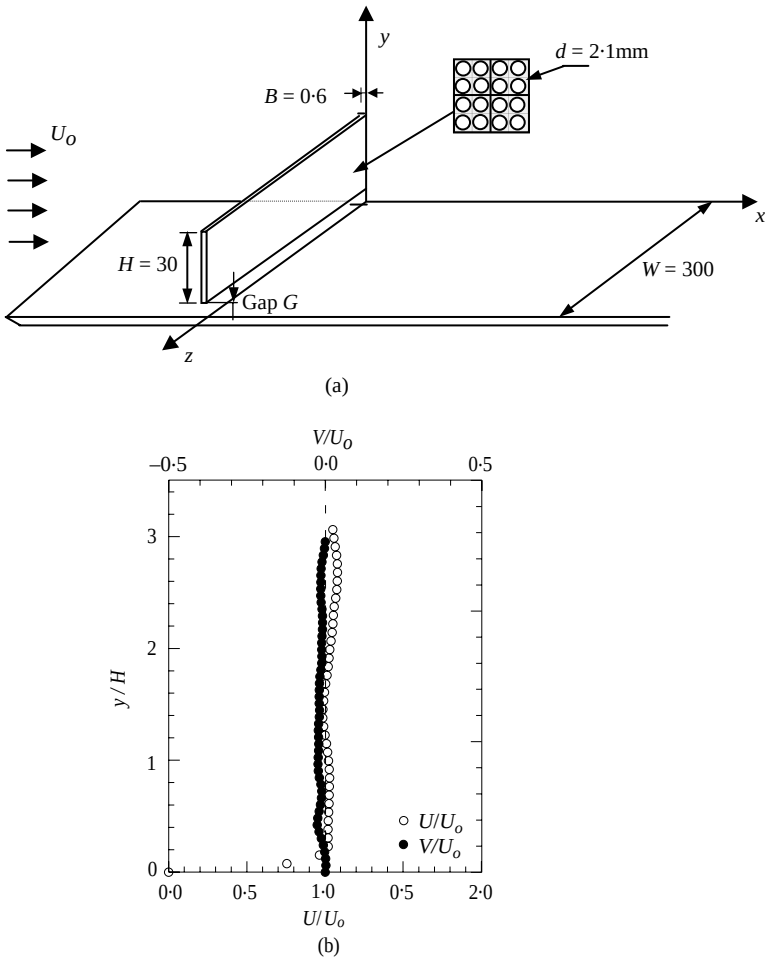

Figure 1. (a) Experimental set-up (all numerical values in mm). (b) Free-stream flow condition at $x/H = -0{\cdot}5$).

a 200 Hz sampling rate. From these pressure measurements, the time-mean wall-pressure shows almost no gradient along the spanwise direction.

The hybrid PTV velocity field measurement technique was implemented in this study to measure the velocity field around the porous fence. A schematic diagram of the PTV velocity field measurement system is given in Figure 2. It consists of a laser light sheet, a high-speed CCD camera (SpeedCam$^+$) and an IBM PC with a frame grabber board.

A thin laser light sheet of approximately 3 mm thickness was formed by passing the laser beam from a 4 W Argon-ion laser through a mirror and a cylindrical lens. Polystyrene particles with a mean diameter of about 85 μm were seeded into the working fluid as tracer particles. Virant & Dracos (1996) have mentioned that seeding particles more than 100 μm in diameter show some discrepancies between fluid and particle motion. Since our particle diameter is less than this criterion and the velocity in the wake region is less than 0·1 m/s, the tracer particles used in our experiment can be assumed to provide a good tracking of the fluid motion. The velocity field measurements were carried out at three consecutive sections behind the fence along the central plane of the water channel to cover the complete x–y

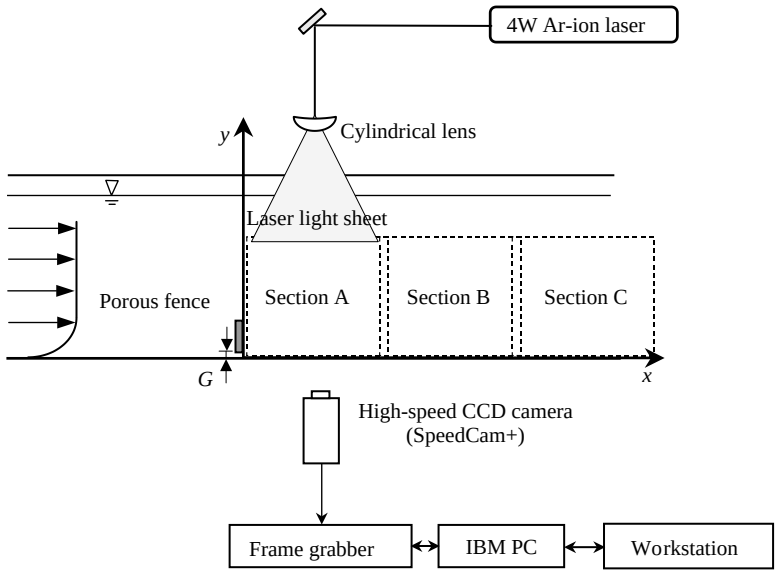

Figure 2. Schematic diagram of the hybrid PTV velocity field measurement system.

plane. The field of view of each cross-section was approximately 60×60 mm. The rear edge of the front section was overlapped about 10 mm with the front edge of the next section.

The flow images were captured using a high-speed CCD camera which can capture flow images at a sampling rate of 1 000 fps (frames per second) with a full resolution of 512×512 pixels. For each measurement section, a total of 1 000 instantaneous flow images were acquired consecutively at 200 fps for 5 s. To obtain tracking velocity vectors from the captured particle images, an adaptive hybrid PTV technique based on the 2-frame PTV algorithm (Baek & Lee 1996) was employed. The difference of mean velocity data between the 2-frame PTV method and LDV under the same flow conditions was found to give less than 1%. The hybrid PTV technique recovers more velocity vectors and decreases the computation time-and-error vectors, compared to the original 2-frame PTV method. Details of the hybrid PTV velocity field measurement technique are described by Kim & Lee (2000).

The instantaneous velocity vectors at the random particle locations were interpolated into a regularly spaced grid using a multi-quadratic interpolation method. The mean velocity field was obtained by ensemble averaging the 1 000 instantaneous velocity vector fields on the grid points (50×50 grids). The interpolated velocity vectors were smoothed using a Gaussian weighting function. However, the smoothing process was minimized to prevent attenuation of peak values and slopes, and the effect of smoothing was checked. The fluctuating velocity vector fields were obtained by subtracting the mean velocity field from the instantaneous velocity fields. All the fluctuating velocity fields were statistically ensemble-averaged to get turbulence statistics including the turbulence intensities, Reynolds shear stress and turbulent kinetic energy. The turbulent kinetic energy $\frac{1}{2}q^2$ was estimated using the following isotropic flow assumption:

$$\tfrac{1}{2}q^2 = \tfrac{1}{2}(\overline{u'^2} + \overline{v'^2} + \overline{w'^2}) \simeq \tfrac{3}{4}(\overline{u'^2} + \overline{v'^2}). \tag{1}$$

Therefore, the actual turbulent kinetic energy will be a little different from the present results in the regions near the top and bottom edges of the fence, where the isotropic assumption is not fulfilled.

3. RESULTS AND DISCUSSION

3.1. Mean Flow Structure

Figure 3 shows the instantaneous velocity vector fields around the porous fence of porosity of $\varepsilon = 38{\cdot}5\%$ for various gap ratios (G/H). Since the fence support blocked the optical ray from particle scattering of the laser light sheet, it was difficult to derive velocity vectors in the region just above the top of the fence. The oncoming flow is divided into two directions in front of the fence; one moves upward and passes over the fence top and the other goes downward and passes through the bottom gap between the lower edge of the fence and the bottom plate. There is no distinct recirculation flow behind the porous fence, irrespective of the gap ratio. The velocity reduction by the porous fence is dominant and clear in the near wake behind the fence. As the gap size increases, the gap flow passing through the bottom gap becomes strong. As the flow goes downstream, the region affected by the gap flow gradually expands.

Figure 4 represents the mean streamwise and vertical velocity profiles taken from Figure 3 at a location of $x/H = -0{\cdot}5$ upstream. The velocity profiles are greatly changed by the existence of the porous fence, compared to the uniform velocity profiles (Figure 1(b)) measured without the fence at the same location. In the upper region, above $y/H \geq 1$, the streamwise velocity decreases as the gap ratio increases. However, in the lower region, below $y/H \geq 1$, the gap ratio of $G/H = 0{\cdot}2$ shows the smallest velocity reduction and the $G/H = 0{\cdot}3$ gap has the largest velocity reduction. For the gap of $G/H = 0{\cdot}1$, the velocity profile is nearly the same as for no gap case ($G/H = 0$).

The vertical velocity profiles have negative values in the region below the mid-height of the fence. With increasing gap size, the negative values of the vertical velocity component increase and the positive values decrease. In addition, the zero-crossing point moves upward. This indicates that the oncoming flow is divided into two opposite directions at the mid-height of the fence. Due to existence of the ground surface, the magnitude of the negative vertical velocity is smaller than that of the positive vertical velocity. The $G/H = 0{\cdot}3$ fence shows that the largest negative value and the downward flow motion in the lower region is more or less comparable with the upward flow motion that passes over the top of the fence.

Figure 5 shows the mean streamwise and vertical velocity profiles selected from the mean velocity field at five downstream locations. In addition to the upper shear layer developed from the fence top, another shear layer is developed from the bottom gap. The mean streamwise velocity increases in the gap space as the gap ratio increases. However, when the gap ratio is larger than $G/H = 0{\cdot}2$, the maximum streamwise velocity in the lower shear layer is nearly unchanged, despite the increase in the gap. In the region of bleed flow passing through the fence holes, the streamwise velocities have nearly the same values regardless of the gap size. This indicates that the mean velocity reduction in the near wake just behind the fence is nearly independent of the gap size. Due to expansion of the shear layers separated from the top and bottom edges of the fence, the region that has a near-uniform velocity profile behind the fence decreases as the flow goes downstream.

For the vertical velocity component, the difference in the velocity profiles with respect to the gap size is not great. Just behind the fence at $x/H = 1$, the vertical velocities have negative values in the bottom gap region for the large gap $G/H = 0{\cdot}3$. This means that the negative vertical velocity component in front of the fence is maintained up to this location, as shown in Figure 3. For the cases of smaller gap ratios, since the gap flow has a smaller momentum and the boundary layer is developing along the bottom surface, it is difficult to see the negative vertical velocity. The vertical velocity component initially increases in the fence top region. The difference between the vertical velocity profiles at the different gap

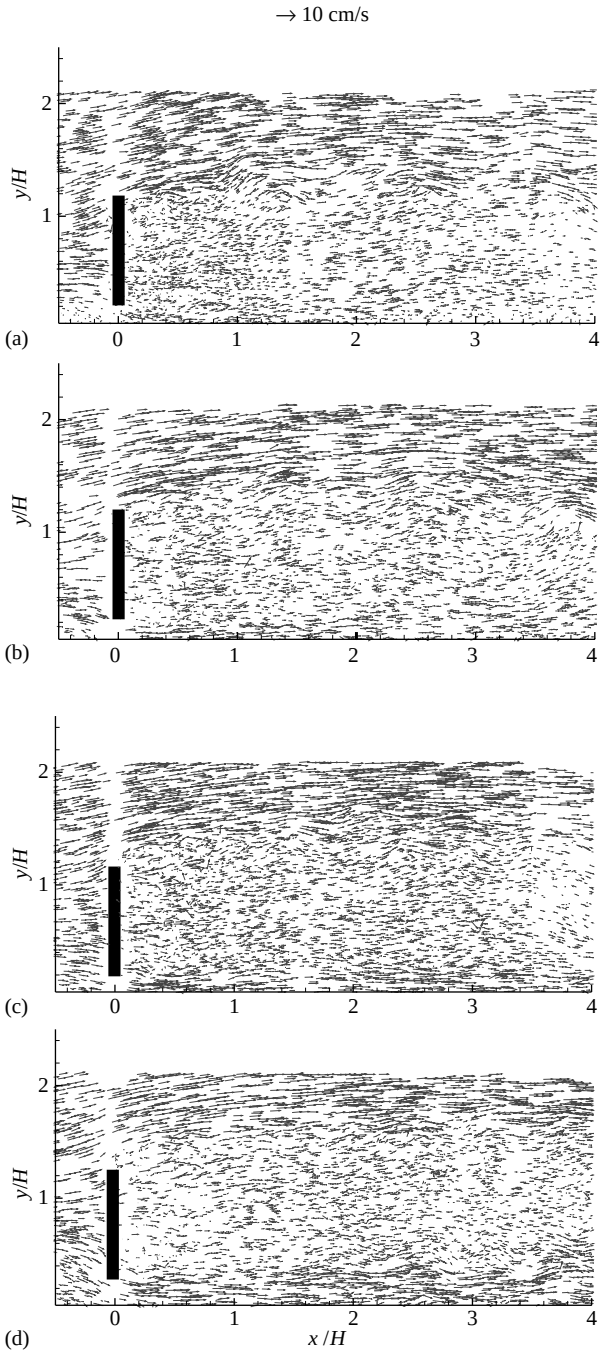

Figure 3. Instantaneous velocity vector fields around a porous fence ($\varepsilon = 38{\cdot}5\%$), measured using the hybrid PTV system: (a) $G/H = 0$; (b) $G/H = 0{\cdot}1$; (c) $G/H = 0{\cdot}2$; (d) $G/H = 0{\cdot}3$.

ratios is reduced as the flow goes downstream in the region $x/H \leq 3$. However, the difference increases again downstream of $x/H = 3$. This may result from the fact that the two shear layers developing from the fence top and gap space start to interact with each

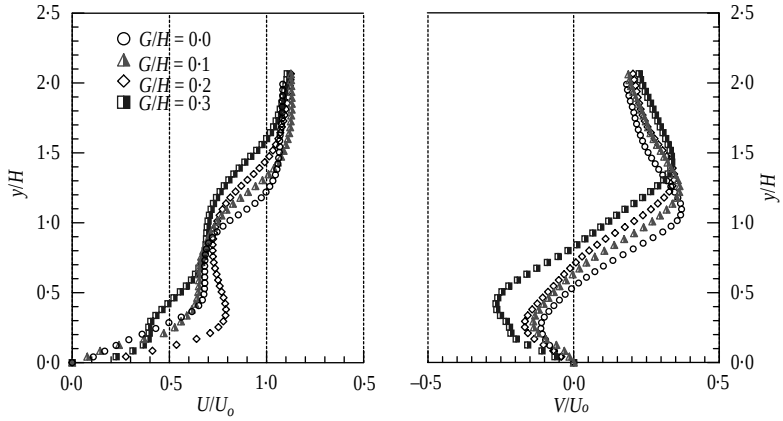

Figure 4. Mean streamwise and vertical velocity profiles at $x/H = -0.5$.

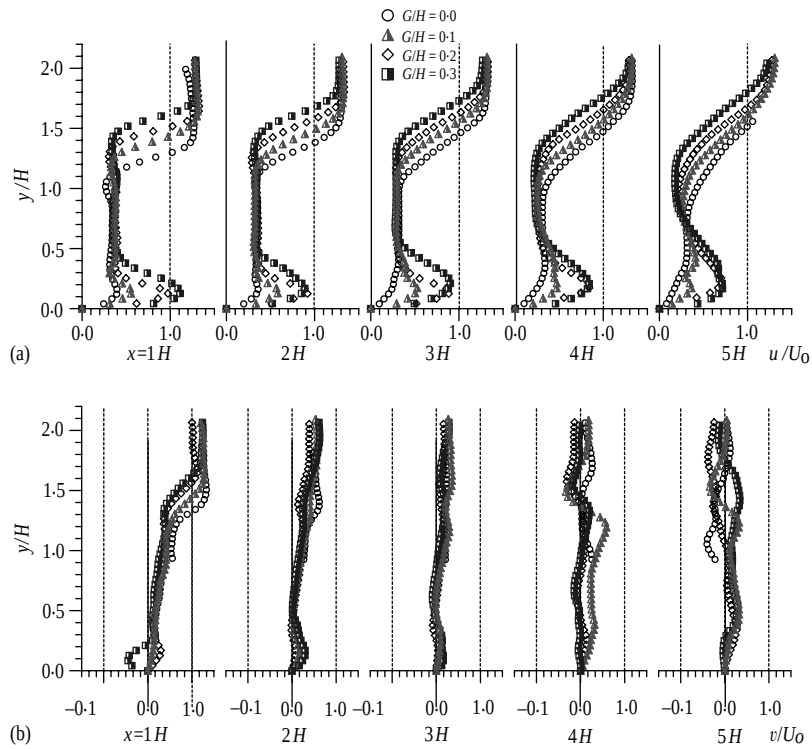

Figure 5. Variations of (a) mean streamwise and (b) mean vertical velocity profiles.

other from the downstream location of $x/H = 4$, as shown in Figure 5(a). For the gap ratio $G/H = 0{\cdot}3$, the vertical velocity profile at $x/H = 5$ is nearly symmetric with respect to the mid-height of the fence.

The variations in velocity ratio (U_{ml}/U_{mu}) between the maximum streamwise velocities at the lower shear layer (U_{ml}) and the upper shear layer (U_{mu}) are shown in Figure 6. For the gap ratio $G/H = 0{\cdot}3$, the maximum velocity (U_{mu}) at the upper shear layer exists outside the

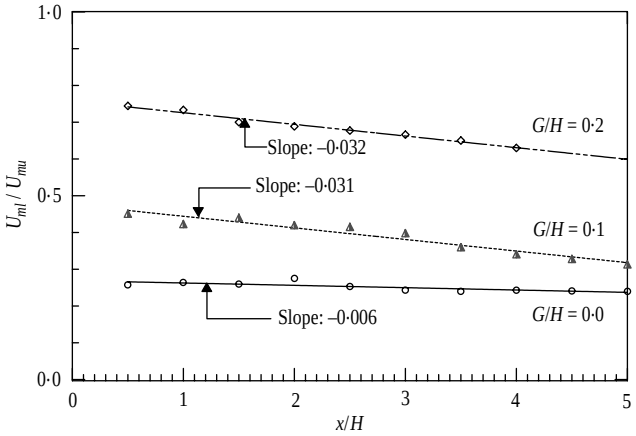

Figure 6. Variations of the maximum streamwise velocity ratio (U_{ml}/U_{mu}) of the upper and lower shear layers.

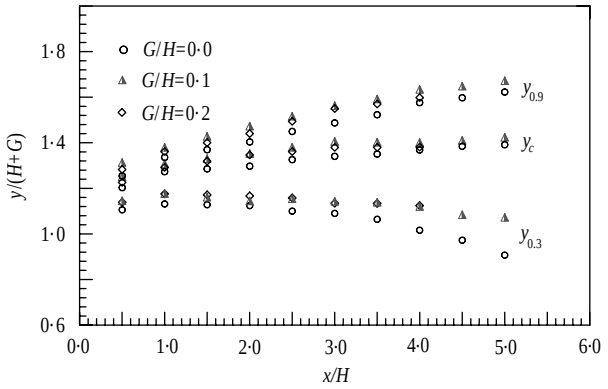

Figure 7. Comparison of the centre-line y_c and boundaries $y_{0\cdot3}$, $y_{0\cdot9}$ of the upper shear layer separated from the fence top.

measurement range tested in this study, as shown in Figure 5(a). The results for no gap ($G/H = 0$) are also included for comparison, for which the streamwise velocity at mid-height of the fence $U_{y/H=0\cdot5}$ was used instead of U_{ml}. The maximum velocity ratio increases as the gap size increases. This results from the increase in streamwise velocity in the lower shear layer with increasing gap size, while the maximum velocity in the upper shear layer is nearly unchanged. As the flow goes downstream, the maximum velocity ratio decreases linearly due to the development of a wall boundary layer and momentum transfer to the bleed flow. The slopes of the decreasing velocity ratio are $-0\cdot031$ and $-0\cdot032$ for the gap ratios of $G/H = 0\cdot1$ and $0\cdot2$, respectively. From this, we can see that the decreasing slope is hardly affected by the gap ratio. For the case with no bottom gap ($G/H = 0$), the velocity ratio has a constant value of approximately 0·28, i.e. the rate of decrease is almost zero. This may result from the existence of a nearly flat velocity profile in the wake flow region.

As the flow goes downstream, both shear layers spread. By analogy with the plane mixing layer, the centre-line of a shear layer can be depicted as a line along which the mean velocity is ($0\cdot67\Delta U + U_{\min}$) (Castro & Haque 1987). Figure 7 shows variations of the centre-line y_c ($= y_{0\cdot67}$) and the boundaries $y_{0\cdot9}$, $y_{0\cdot3}$ of the upper shear layer. Here, $y_{0.3}$, y_c and

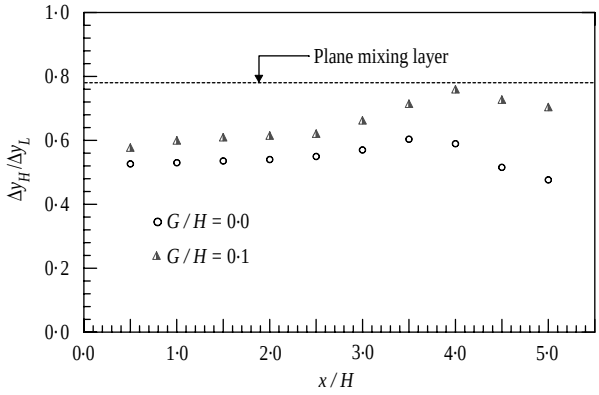

Figure 8. Thickness ratio between the upper and lower sides of the upper shear layer.

$y_{0\cdot9}$ indicate the locations at which $U/U_{\max}$ is equal to 0·3, 0·67 and 0·9, respectively. The lower boundary of the shear layer is usually expressed as $y_{0\cdot1}$. However, since the bleed flow behind the fence has a higher streamwise velocity than that for $y_{0\cdot1}$, the quantity $y_{0\cdot3}$ was used to depict the lower boundary of the shear layer.

The upper shear layer, separated from the fence top, grows as the flow goes downstream. For comparison, the y-axis was nondimensionalized by the combined height $(H + G)$ of the fence and gap. Since the maximum velocity for $G/H = 0{\cdot}3$ was located outside the measurement range, the corresponding results were excluded from Figure 7. For the same reason, the boundaries $y_{0\cdot9}$ for the $G/H = 0{\cdot}2$ gap ratio were plotted only up to the downstream location of $x/H = 4$. The porous fence with no bottom gap $(G/H = 0)$ has the lowest shear layer boundaries $y_{0\cdot3}$, y_c and $y_{0\cdot9}$.

The fence gap effect is clearly shown in the lower boundary $(y_{0\cdot3})$ of the shear layer. As the flow goes downstream, the difference in the boundary locations with and without the bottom gap increases. However, the centre and upper boundaries $(y_c, y_{0\cdot9})$ of the shear layer do not show this kind of large variation.

The upper and lower sides of the shear layer are commonly represented by the thicknesses $\Delta y_H = (y_{0\cdot95} - y_c)$ and $\Delta y_L = (y_c - y_{0\cdot2})$, respectively. As mentioned earlier, however, in this experiment $y_{0\cdot9}$ and $y_{0\cdot3}$ were used instead of $y_{0\cdot95}$ and $y_{0\cdot2}$. Therefore, an exact comparison of the absolute values with those of the plane mixing layer is not possible; however, it is possible to compare their trend. Figure 8 shows the thickness ratio $(\Delta y_H/\Delta y_L)$ between the upper and lower sides of the upper shear layer. The thickness ratio $\Delta y_H/\Delta y_L$ is nearly constant up to the downstream location of $x/H = 3$, where the two shear layers start to interact. Thereafter it increases and has a peak value at around $x/H = 3{\cdot}5$–$4{\cdot}0$ and then decreases again. The thickness ratio for the gap ratio $G/H = 0{\cdot}1$ is larger than that for the no-gap case. The difference in the thickness ratios for the gap ratios of $G/H = 0$ and 0·1 increases as one goes downstream. This indicates that the lower side thickness Δy_L for the gap ratio $G/H = 0$ is larger than that for the gap ratio $G/H = 0{\cdot}1$.

3.2. Turbulence Structure

The normalized r.m.s. turbulence profiles of the streamwise and vertical velocity components $(\sqrt{u'^2}/U_0, \sqrt{v'^2}/U_0)$ are given in Figure 9. For all test conditions, the turbulence intensities have maximum values at the shear layers developed from the fence top and the bottom gap. The maximum streamwise turbulence intensity $\sqrt{u'^2}/U_0$ has similar values in

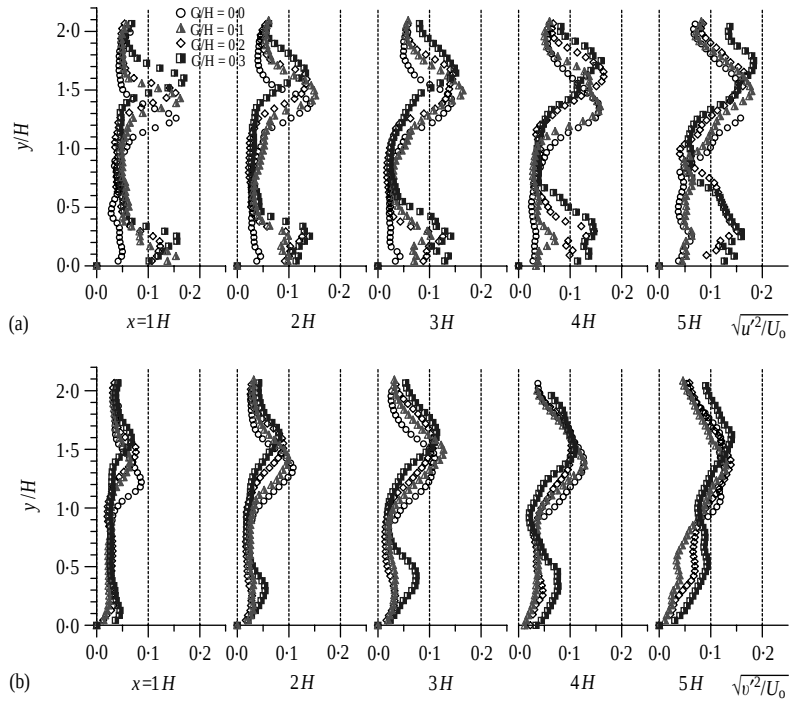

Figure 9. (a) Streamwise and (b) vertical turbulence intensity profiles.

the upper shear layer regardless of the gap ratio. The location of the local maximum turbulence intensity moves upward as the gap ratio increases.

The lower shear layer shows a little difference in the turbulence structure, compared to the upper shear layer. The maximum turbulence intensity increases as the gap ratio increases. The region displaying large turbulence intensity values expands as the flow goes downstream due to the expansion of the shear layer. The turbulence intensity profiles for the porous fence with gap ratio $G/H = 0{\cdot}1$ become similar to those of the no-gap case as the flow goes downstream. Momentum transfer to the bleed flow and the development of a wall boundary layer seem to make the lower shear layer rapidly disappear for the gap ratio $G/H = 0{\cdot}1$. When the gap ratio is greater than $G/H = 0{\cdot}2$, the streamwise turbulence intensity profiles show two peaks in the lower shear layer. This may be attributed to the interaction between the wall boundary layer and the shear layer separated from the bottom edge of the fence. For the gap ratio $G/H = 0{\cdot}2$, the maximum turbulence intensities in the upper and lower shear layers have similar values and show only a 3% difference at the location $x/H = 1$, just behind the fence.

Figure 9(b) shows the vertical turbulence intensity profiles. In the upper shear layer, the magnitude and general shape of the vertical intensity profiles are similar irrespective of the gap ratio. However, in the lower shear layer, only the $G/H = 0{\cdot}3$ gap fence has large values up to the downstream region of $x/H \leq 3$. Thereafter, the vertical turbulence intensity increases in the lower shear layer as the gap ratio increases.

From these results, we can see that the vertical velocity fluctuations in the lower shear layer are much smaller than those of the upper shear layer due to the existence of the wall. However, the streamwise velocity fluctuations in both lower and upper shear layers have similar maximum values when the gap size is larger than $G/H = 0{\cdot}1$.

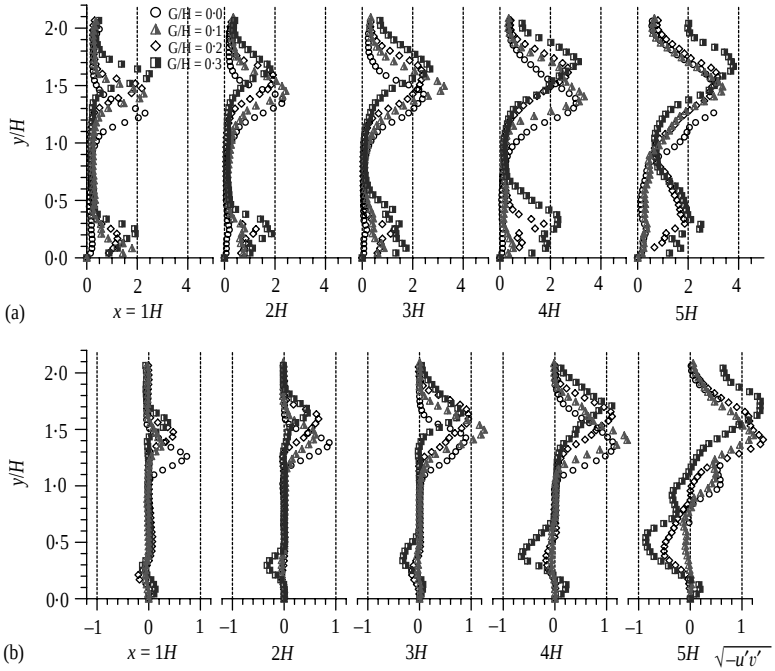

Figure 10. (a) Turbulence kinetic energy and (b) Reynolds shear stress profiles.

The turbulent kinetic energy $\frac{1}{2}q^2$ and Reynolds shear stress ($-\overline{u'v'}$) profiles at five downstream locations are shown in Figure 10. As can be expected from Figure 9, in the centre region of both shear layers the turbulent kinetic energy has a high value. The general shape of the kinetic energy profiles is similar to that in the streamwise turbulence intensity profiles. The location of the maximum kinetic energy in the upper shear layer moves upward as the gap ratio increases. However, in the lower shear layer the turbulence kinetic energy profiles show a drastic change in behaviour depending on the bottom gap size. For the gap ratios larger than $G/H = 0{\cdot}2$, the lower shear layer has a high turbulence kinetic energy up to the end of the measurement range. For the small gap ratio $G/H = 0{\cdot}1$, the flow has a small kinetic energy in the near wake region for $x/H < 3$, thereafter the kinetic energy has a profile similar to that of the no bottom gap case. Due to the small vertical turbulence intensity in the lower shear layer, the turbulent kinetic energy has smaller values in this layer compared to the upper shear layer.

The Reynolds shear stress ($-\overline{u'v'}$) has larger values in the upper shear layer than that of the lower shear layer. In the lower shear layer, only the $G/H = 0{\cdot}3$ fence has significant Reynolds shear stress values up to $x/H = 4$. At $x/H = 5$, the porous fence with $G/H = 0{\cdot}2$ also displays relatively large shear stress values in the lower shear layer.

Consequently, the turbulence statistics including turbulence intensities, Reynolds shear stress and turbulent kinetic energy have similar profiles and local maximum values in the upper shear layer, irrespective of the gap ratio. However, in the lower shear layer developed from the bottom gap, the turbulence statistics for the gap ratio of $G/H = 0{\cdot}1$ have much smaller values compared to the larger gap ratios of $G/H = 0{\cdot}2$ and $0{\cdot}3$, displaying a turbulence structure similar to that of the same porous fence without a bottom gap ($G/H = 0$).

Gandemer (Perera 1981) has proposed a shelter parameter to quantify the sheltering effect of the wall. However, this parameter reflected only the streamwise mean velocity and

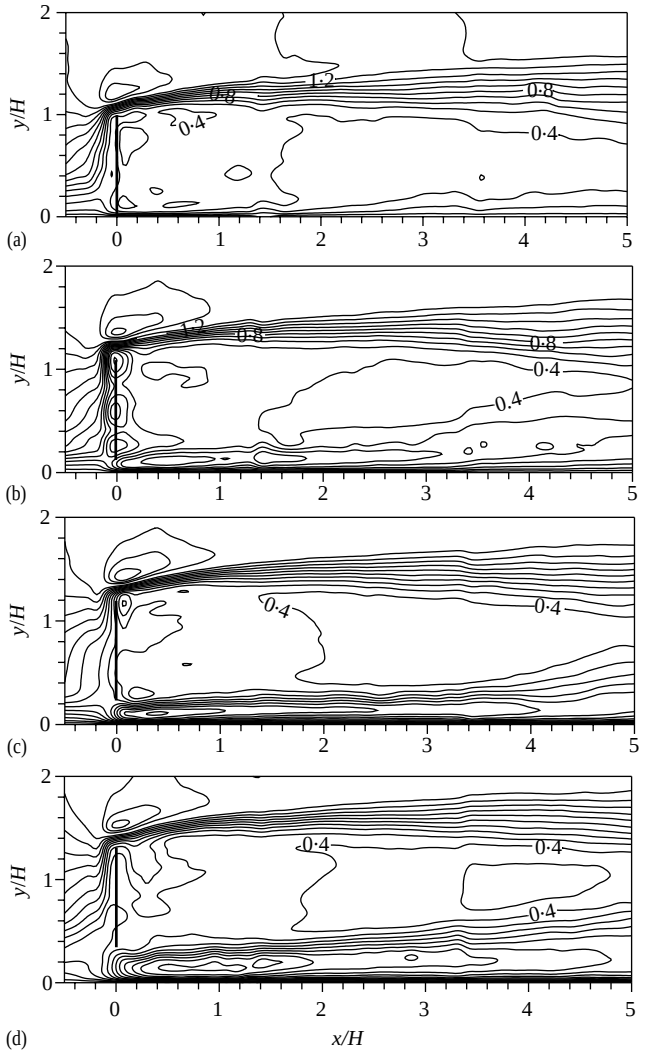

Figure 11. Shelter parameter contours with various gap sizes: (a) $G/H = 0$; (b) $G/H = 0{\cdot}1$; (c) $G/H = 0{\cdot}2$; (d) $G/H = 0{\cdot}3$.

turbulence intensity. Although the vertical velocity component is relatively small compared to the streamwise velocity component, it must be considered in addition to the streamwise velocity component to obtain an accurate shelter parameter. Therefore, in this study, a modified shelter parameter, ψ, that takes into account both the streamwise and vertical velocity components, was defined as follows:

$$\psi = \frac{(|U| + \sqrt{u'^2} + |V| + \sqrt{v'^2})}{(U_0 + \sqrt{u_0'^2})}. \tag{2}$$

Figure 11 shows contour plots of the shelter parameter as a function of the gap ratio. The shelter parameter ψ in the upper shear layer shows similar contours irrespective of the gap ratio. The region displaying significant values expands as the flow goes downstream. In the lower shear layer, the shelter parameter ψ increases and the region with large ψ values

expands as the gap ratio increases. The shelter parameter in the bleed flow region just behind the fence has small values. For the gap ratio $G/H = 0{\cdot}3$, the large gap flow through the bottom gap makes the region with small ψ values move upward. The porous fence with gap ratio $G/H = 0{\cdot}1$ gives a good shelter effect, similar to that of the no-gap fence.

4. CONCLUSION

The flow behind a porous fence with a bottom gap can be divided into three regions: an upper shear layer separated from the fence top, a bleed flow passing through the fence holes, and a lower shear layer developed from the bottom gap.

The upper boundary of the upper shear layer has a shape almost independent of the gap ratio. However, the lower boundary of the upper shear layer moves upward as the gap ratio increases, because the lower shear layer expands and pushes the lower side of the upper shear layer upward. For the gap ratio $G/H = 0{\cdot}1$, the lower shear layer disappears in the region downstream of $x/H \geq 3$ and the mean velocity is reduced in the large region behind the fence.

For the gap ratio $G/H \geq 0{\cdot}2$, the turbulence statistics including turbulence intensities, Reynolds shear stress and turbulent kinetic energy have large values in the lower shear layer developed from the bottom gap. However, for the gap ratio $G/H = 0{\cdot}1$, the turbulence statistics have small values and as the flow goes downstream they approach those of the no-gap case. This may be attributed to the small momentum of the gap flow and momentum transfer to the bleed flow region.

The general shape of the turbulence intensity profiles in the upper shear layer is similar irrespective of the gap ratio. The vertical turbulence intensity and turbulence kinetic energy in the lower shear layer are much smaller than those of the upper shear layer. In the lower shear layer, the shelter parameter ψ representing the adverse shelter effect increases as the gap ratio increases. The $G/H = 0{\cdot}1$ gap fence also gives a good shelter effect similar to that of the no-gap fence in the large wake region behind the fence.

References

Baek, S. J. & Lee, S. J. 1996 A new two-frame particle tracking algorithm using match probability. *Experiments in Fluids* **22,** 23–32.

Castro, I. P. & Haque, A. 1987 The structure of turbulent shear layer bounding a separation region. *Journal of Fluid Mechanics* **179,** 439–468.

Castro, I. P. 1971 Wake characteristics of two-dimensional perforated plates normal to an air-stream. *Journal of Fluid Mechanics* **46,** 599–609.

Cho, H. M. 1996 Wind-tunnel and numerical simulation of flow over porous fences and particle saltation in atmospheric boundary layer. Ph.D. dissertation, Department of Mechanical and Aeronautical Engineering, University of California at Davis, Davis, CA, U.S.A.

Kim, H. B. & Lee, S. J. 2000 Performance improvement of 2-frame PTV method using an adaptive hybrid scheme. *KSME Journal* **24,** 443–449.

Kim, H. B. & Lee, S. J. 2001 Hole diameter effect on flow characteristics of wake behind porous fences having the same porosity. *Fluid Dynamic Research* **28,** 449–464.

Lee, S. J. & Kim, H. B. 1999 Laboratory measurements of velocity and turbulence field behind porous fences. *Journal of Wind Engineering and Industrial Aerodynamics* **80,** 311–326.

Perera, M. D. A. E. S. 1981 Shelter behind two-dimensional solid and porous fences. *Journal of Wind Engineering and Industrial Aerodynamics* **8,** 93–104.

Raine, J. K. & Stevenson, D. C. 1977 Wind protection by model fences in simulated atmospheric boundary layer. *Journal of Wind Engineering and Industrial Aerodynamics* **2,** 159–180.

Virant, M. & Dracos, Th. 1996 In *Three-dimensional Velocity and Vorticity Measuring and Image Analysis Techniques* (ed. Th. Dracos). Dordrecht: Kluwer Academic Pub.